

# Refractories Applications *Transactions*

Volume 3, Number 1

July/August 2007

## Editorial Board

Jeffrey D. Smith, Editor, University of Missouri-Rolla, USA  
Mary Lee, Assistant to the Editor, University of Missouri-Rolla, USA  
William Headrick, University of Missouri-Rolla, USA  
Musa Karakus, University of Missouri-Rolla, USA

## Technical Referees

**Esteban Aglietti**, CETMC, Argentina  
**Richard C. Bradt**, The University of Alabama, USA  
**Carmen Baudín**, Instituto de Cerámica y Vidrio, Spain  
**Elena Brandaleze**, Instituto Argentino de Siderurgia  
**Angel Caballero**, Instituto de Cerámica y Vidrio, Madrid, Spain  
**William G. Fahrenholtz**, University of Missouri-Rolla, USA  
**Geraldo E. Gonçalves**, Magnesita S.A., Brazil  
**Orville Hunter**, Consultant, USA  
**William E. Lee**, University of Sheffield, UK  
**Li Nan**, Wuhan University of Sci. & Tech., China  
**George Oprea**, The University of British Columbia, Canada  
**Victor C. Pandolfelli**, Universidade Federal de São Carlos, Brazil  
**Christopher Parr**, Lafarge Aluminates, France  
**Jacques Poirier**, Polytech, Orleans, France  
**Michel Rigaud**, Ecole Polytechnique, Canada  
**Charles Semler**, Semler Materials Services, USA  
**Mark Stett**, Consultant, USA  
**Raul Topolevsky**, Siderar, Argentina

All submissions should be sent to:

**Mary Lee, Assistant to the Editor**  
**Refractories Applications Transactions**  
**University of Missouri-Rolla**  
**Materials Science and Engineering Dept.**  
**223 McNutt Hall**  
**1870 Miner Circle Drive**  
**Rolla, MO 65409-0330**

**Phone: (573) 341-6561**  
**Fax: (573) 341-6934**  
**E-mail: leem@umr.edu**

For author guidelines please see those listed on the *Journal of the American Ceramic Society* website: <http://www.ceramics.org/publications/journal/authorinstructions.asp>

File Formats

Text: Microsoft Word.

Graphics: JPEG, TIFF or EPS created from supported applications, PowerPoint, Acrobat PDF (PDF format is acceptable for review purposes only)

Microsoft Word with embedded graphics.

Compression Software: WinZip (PC) or Stuffit (Macintosh)

Resolution of graphics files must be at least 300 dpi for halftones, 600 dpi for lettering, and 1200 dpi for line art.

## Interaction of Molten Ultra-Low Carbon Steel with Carbide and Nitride Refractory Materials

Robert B. Tuttle<sup>‡</sup>, Kent D. Peaslee<sup>†</sup> And Jeffrey D. Smith<sup>†</sup>

<sup>‡</sup>Department Of Mechanical Engineering, Saginaw Valley State University

<sup>†</sup> Department Of Materials Science And Engineering, University Of Missouri-Rolla, Rolla, Mo 65409

*kpeaslee@umr.edu*

### ABSTRACT

Nozzle clogging of tundish and submerged entry nozzles causes low productivity and inferior quality during continuous casting of aluminum-killed steels. Clogging is caused by an accretion layer that forms on the inside surface of the nozzle orifice restricting flow of the liquid steel. The current generation of refractory materials is known to react with molten steel forming products in the nozzle orifice that can increase the clogging process. Nozzle materials that are either inert with liquid steel or prevent the attachment of inclusions decrease clogging. In the present investigation, molten steels containing different levels of aluminum were placed in contact with boron nitride, silicon carbide, and boron carbide to evaluate these materials as potential nozzle refractories. The contact surfaces between the refractory and steel were examined using reflected light, cathodoluminescence, and scanning electron microscopy. All three materials reacted with molten steel. Both boron nitride and boron carbide reacted with molten steel to form metallic iron and iron boride. On the other hand, the silicon carbide reacted with molten steel to form iron and iron silicide. Silicon carbide and boron carbide reacted more extensively with molten steel than boron nitride.

### INTRODUCTION

Aluminum-killed steels routinely undergo clogging in the tundish well and submerged entry nozzle (SEN) during continuous casting. The clogging starts when alumina accretions form on the nozzle wall and obstruct the flow of steel. Typically, the accretion layer grows throughout a casting sequence resulting in frequent nozzle changes or in more severe cases, termination of the cast. Portions of the accretion layer often detach and enter the steel stream where they can cause quality problems. As the accretion grows, the alumina located near the nozzle wall typically densifies as illustrated in **Figure 1**.<sup>1</sup>

Alumina, which forms the accretions, arises from a number of possible sources. Aluminum is added to the steel to deoxidize the metal resulting in the formation of alumina as a deoxidation product. Most deoxidation products float and are caught by the slag immediately after deoxidation. However, some of the smaller alumina particles are cast along with the steel and can attach to the nozzle surface. In addition, aluminum killed steels contain high levels of soluble aluminum which reacts with oxygen that enters the steel during the casting process to form alumina that can attach to the nozzle surface. On entering the

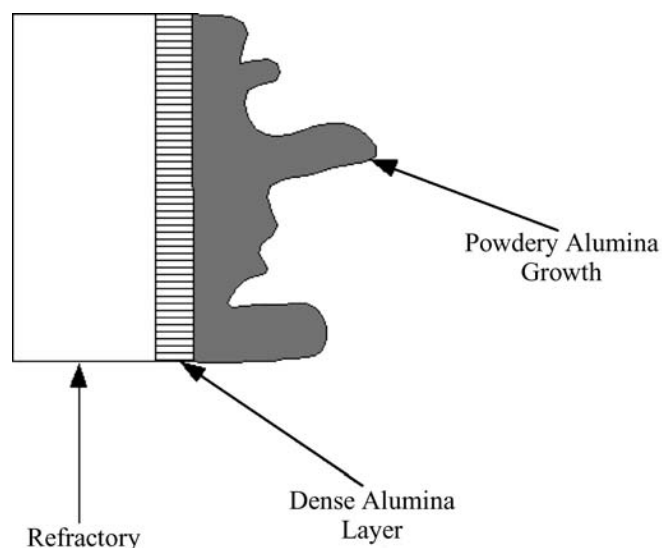


**Fig. 1.** Diagram of accretion structure in alumina-graphite nozzles.

steel, the oxygen reacts with the soluble aluminum if the steel is exposed to air. This can occur during transfer between steelmaking vessels, through leaks in the ladle shroud or SEN, or turbulence during casting.<sup>2</sup> Several refractories produce small amounts of suboxide gasses at steelmaking temperatures.<sup>1,3,4</sup> These suboxide gasses transport themselves to the steel/refractory interface where they react with the soluble aluminum in the steel forming alumina at the nozzle/steel interface.

Changing the type of refractory material could minimize nozzle clogging. One approach would be to use refractories that react with the alumina particles to form a liquid phase that will not attach to the accretion. A second approach, and the one attempted in this study, is to use refractories that do not react with the steel or alumina particles to reduce the possibility of particle attachment and accretion formation. Boron nitride, silicon carbide, and boron carbide were selected as candidate materials. Boron nitride, with a melting point of 3027°C, has been used in several steelmaking applications.<sup>5,6</sup> Silicon carbide, with a dissociation temperature of 2830°C, has found wide application in metalcasting operations, blast furnace refractories, and as kiln furniture.<sup>7</sup> Boron carbide has been used in grinding and nuclear reactor control rod applications.<sup>7</sup> All three materials are known to be chemically stable within their current applications.

To determine the suitability of each material for use in continuous casting, static experiments were conducted in which several different molten steels were placed in contact with the candidate refractories for several hours. Because steel does not flow past the steel/refractory interface in these experiments, the reaction products are preserved at the interface, simplifying reaction product identification.

### EXPERIMENTAL PROCEDURE

Boron nitride, silicon carbide, and boron carbide were obtained from commercial manufacturers that hot press the material to near theoretical density. In each refractory sample, holes, 0.635 cm (1/4-inch) diameter by 2.54 cm (1-inch) depth, were prepared to allow for insertion of steel pins during the experiments. Holes were drilled in the boron nitride samples. Because the silicon carbide and boron carbide samples were supplied with 0.635 cm holes through the entire thickness, 99.9% pure, -325 mesh zirconia powder was placed in the bottom of each hole to contain the steel within the sample during the experiments (see **Figure 2**). Zirconia was selected based on previous work that showed zirconia to be inert with these steels.<sup>8</sup> Two samples were run for each refractory material, one with aluminum-killed steel and a second with unkill steel (see **Table 1**).

During the experiment, the samples were surrounded by an alumina bell and plate in a resistance furnace. Argon gas flowed into the bell and graphite encircled the samples inside the enclosure to reduce the oxygen potential of the atmosphere around the sample (see **Figure 3**). A heating rate of 130°C/hour was used to attain a temperature of 1585°C. The samples were held at this temperature for two hours. After completing the experiment, the furnace was cooled to room temperature under argon in approximately eight hours.

Each sample was removed and vacuum impregnated with low viscosity epoxy resin. After impregnation, the sample was sectioned and mounted for grinding and polishing to a 1-micron finish. Reflected light (RL), cathodoluminescence (CL), and scanning electron microscopy (SEM) were conducted to examine each sample. X-ray diffraction

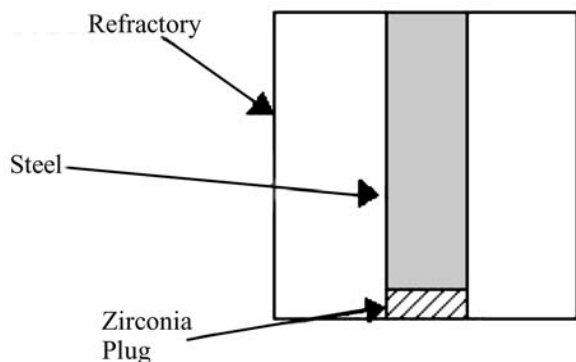


**Fig. 2.** Arrangement of boron carbide and silicon carbide samples.

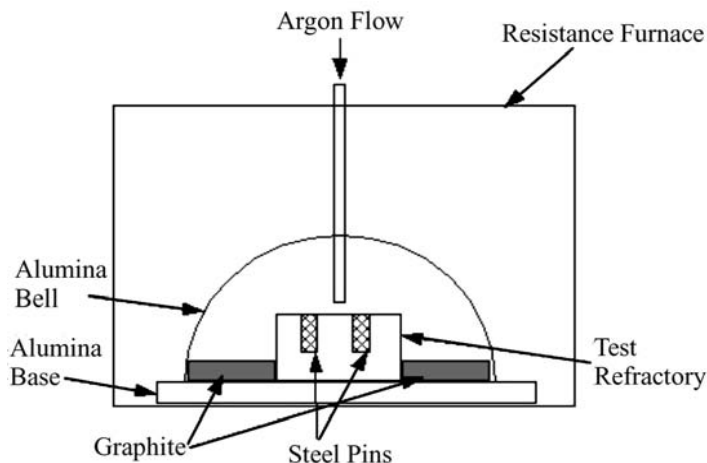


**Fig. 3.** Experimental apparatus arrangement.

(XRD) was also conducted on the samples to determine the phases that formed during the experiment.

Cathodoluminescence (CL) microscopy is an effective characterization tool for metal/ceramic interaction. Ceramic phases are easily identified in CL by their color. However, steel and iron oxides do not luminesce and appear black in CL images. Therefore, it was necessary to take reflective light (RL) images of the interface to accurately capture all the phases at the refractory/steel interface. For all CL images in this paper, the top quarter of the photomicrograph contains a RL image of the area under investigation and the remaining portion contains the CL image.

### RESULTS AND DISCUSSION

Previous work examined the steel/refractory reactions in typical alumina graphite nozzle materials.<sup>9</sup> In this study, alumina accretions and a decarburized zone at the refractory/steel interface were found to be typical for aluminum killed steels. Aside from the accretions, there were very little signs of reaction products detected inside the metal.

#### Boron Nitride

Examination of the refractory/steel interface in the aluminum-killed and unkill steel samples with boron nitride displayed evidence that reactions occurred during the experiment. The characteristic microstructure of the interface is shown in the CL images on right side of the micrographs in **Figures 4 and 5**, unreacted refractory showing yellow grains of zirconia in the blue boron nitride. Since iron does not luminesce, the steel appears black. Zirconia is present in these samples because it is added to commercial boron nitride to aid sintering. A 200  $\mu\text{m}$  wide void was observed in the sample between the steel and refractory, which was caused, by the volume change (liquid to solid steel) and

**Table 1.** Steel pin chemistry

Sample	C (wt%)	Mn (wt%)	Al (wt%)	S (wt%)	P (wt%)	Si (wt%)	Oxygen (ppm)
Unkilled Steel	0.006	<0.01	<0.01	0.006	0.005	<0.01	489
Killed Steel	0.006	<0.01	0.090	0.006	0.004	<0.01	5

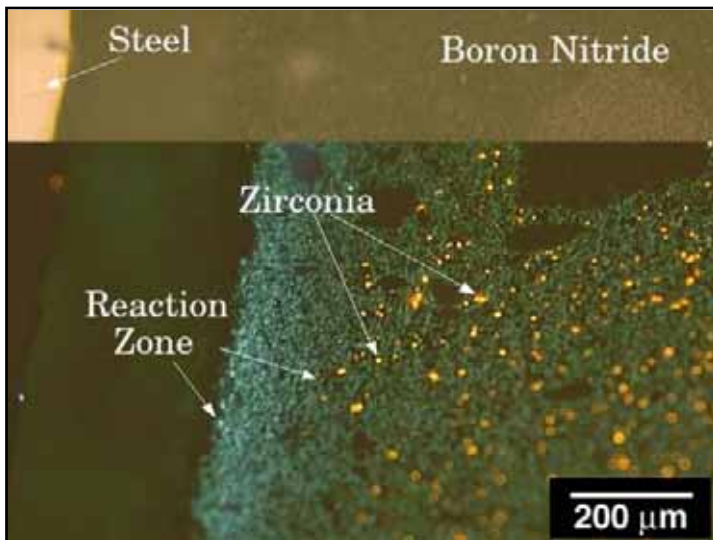


Fig. 4. CL/RL image of the steel/BN interface in the unkilld ULC sample.

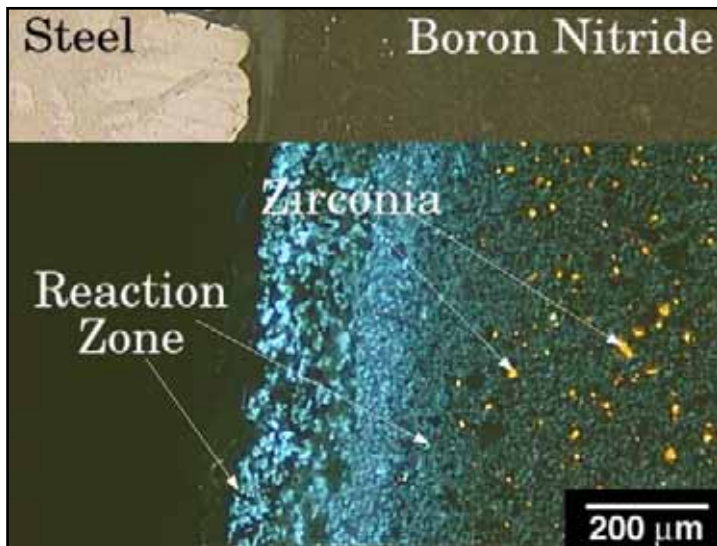


Fig. 5. CL/RL image of the steel/BN interface from the aluminum killed ULC sample.

thermal expansion mismatch between the steel and boron nitride during solidification and cooling. The refractory in contact with the steel contains only boron nitride and is devoid of zirconia grains. The change in color and lack of zirconia indicate that the refractory reacted with the steel. Reaction zones were present in both samples, but differed in appearance. The zirconia-depleted zone in the unkilld sample (Figure 4) is approximate 200  $\mu\text{m}$  in thickness. However, the reaction zone has an additional thickness of 100 microns in the killed steel (Figure 5) where major damage occurred between the zirconia-depleted zone and the steel. Also, reaction zones have been observed by Asano et al. at the refractory/steel interface of stainless steel and boron nitride containing refractories.<sup>6</sup> In this study, it has been observed that the reaction zone size increased with an increase of boron nitride content.

Since the steel appears black in CL, it was examined with RL and SEM. Figure 6 shows the microstructure of the unkilld steel taken at the center of the crucible after the experiment. The microstructure contains ferrite grains, surrounded by a second phase in the grain boundaries, which is distinctly different than the expected ferritic structure of the original ultra low carbon (ULC) unkilld steel pin used for the

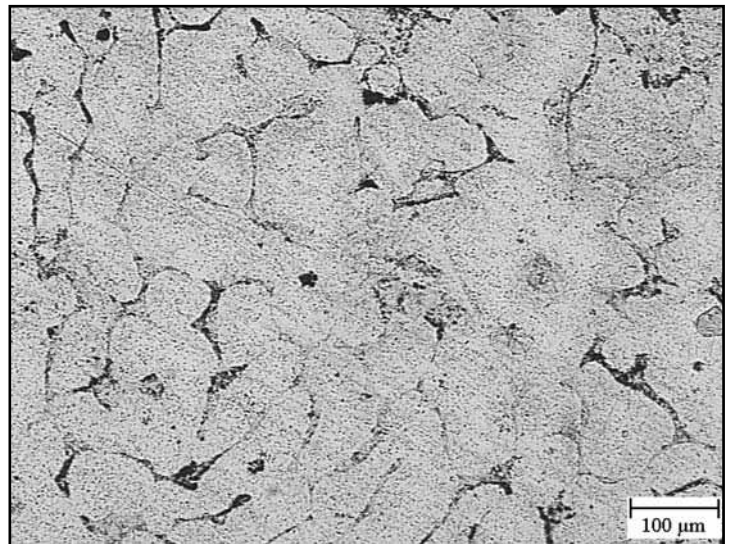


Fig. 6. RL image of the unkilld ULC steel structure in BN.

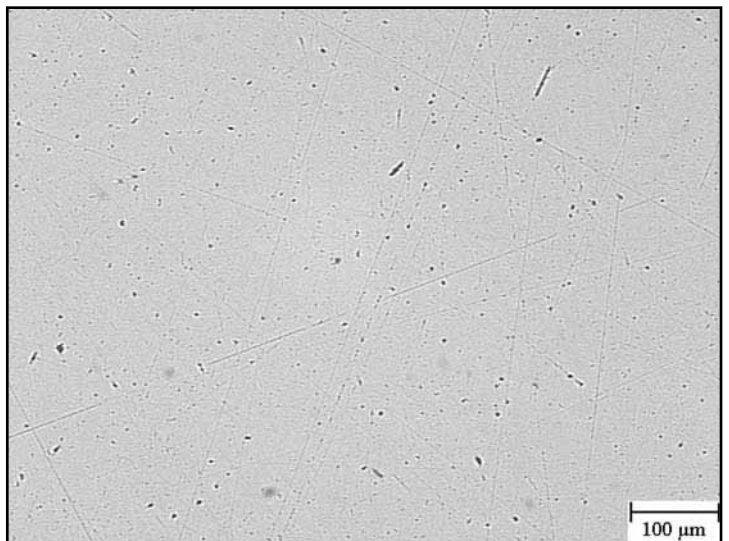


Fig. 7. RL image of unkilld ULC steel.

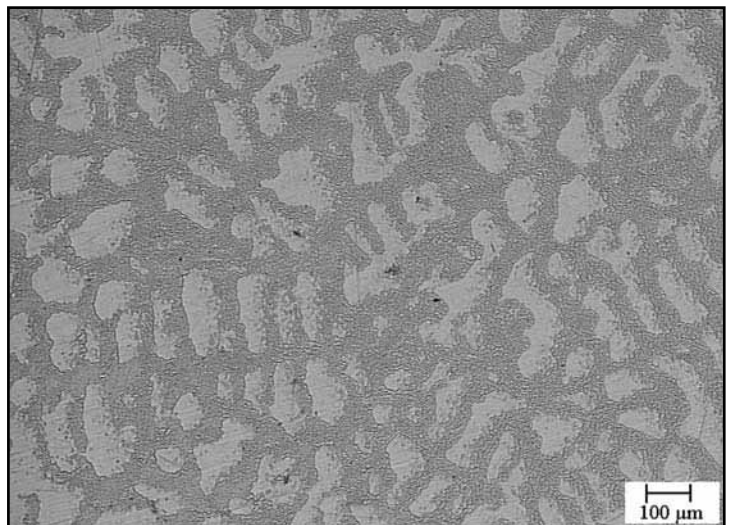


Fig. 8. RL image of the aluminum killed ULC steel structure in BN.

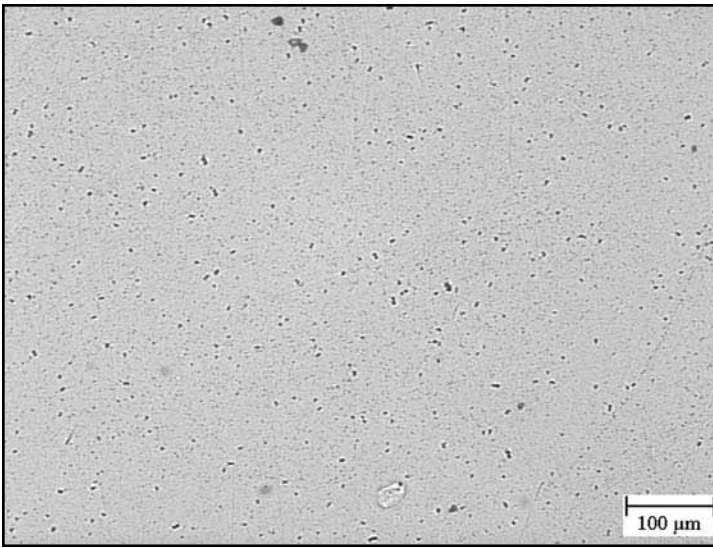


Fig. 9. RL image of aluminum killed ULC steel.

experiments (see **Figure 7**). The change in the microstructure was even more pronounced for the killed ULC steel. In **Figure 8**, ferrite dendrites can be seen surrounded by an interdendritic phase, which is different from the expected ferritic structure for the killed steel microstructure (see **Figure 9**). The interdendritic phase and the phase at the grain boundaries in the unkilld sample as examined under a high magnification indicated that both were of similar structure. In this microstructure, the ferrite grains are surrounded by a second phase, which formed by the contamination of the iron during reactions with the refractory. Because the original steel is nearly pure iron, the microstructure should consist of grains or dendrites of  $\alpha$ -iron with no interdendritic region. Thus, the development of the observed microstructures was caused by the absorption of boron from the boron nitride refractory.

Energy dispersive spectroscopy (EDS) was able to detect the presence of boron in the sample. However, the boron peak intensity was not large enough to enable quantitative analysis. XRD analysis of the steel and refractory identified the presence of iron, boron nitride, and zirconia in the unkilld and killed samples. Peaks corresponding to the phases in the eutectic were most likely obscured by other phases present in the sample and background noise. CL was ineffective in indicating a chemistry change in the metallic phases. Therefore, regardless of the presence of boron in the metallic phases, quantitative boron analysis was not possible using the characterization techniques available in the present study.

In the iron-boron system, two eutectic phases are present. One eutectic is between iron and  $\text{Fe}_2\text{B}$ , and the other is between  $\text{FeB}$  and boron.

The most likely eutectic to form in either sample is the iron- $\text{Fe}_2\text{B}$  eutectic because XRD still detected the presence of iron and only a relatively small amount of boron nitride refractory reacted with the steel. Based on a close examination of the phase diagram, only 0.10 wt% boron is soluble in ferrite before  $\text{Fe}_2\text{B}$  is formed.

Based on the observed microstructure, the boron content of the steel was estimated. Area percentages of the primary iron phase and eutectic present in the optical micrographs were measured by image analysis and used to estimate the volume percentage of each phase in the microstructure. The volume percentages from the micrographs were converted to mass percent of each phase by multiplying by the density of ferrite (for the primary phase) and the density of  $\text{Fe}_2\text{B}$ . The mass percentages were used in a simple lever rule calculation to determine the boron content of each sample. The calculations assume that the eutectic observed was the Fe- $\text{Fe}_2\text{B}$  eutectic with 0.48 wt% boron in the unkilld sample and 2.24 wt% boron for the aluminum-killed sample. FACTSage™, commercially available free-energy minimization software, was used to thermodynamically predict the reaction products that occur between the refractory and iron at 1585°C. A molar ratio of 1 mole BN: 50 moles steel was used as the input materials based on the observed ratio of reaction layer to steel in the samples. **Table 2** lists the input moles for the model based on thermodynamic standard states, iron, carbon, aluminum and BN were input as solids and argon and carbon monoxide were input as gases. Results from the thermodynamic calculations are listed in **Table 3**. The results predict that nearly all of the boron and approximately half of the nitrogen dissolves into the steel. The remainder of the nitrogen accumulated in the argon atmosphere, assumed to contain  $10^{-5}$  atm. of CO due to the presence of the graphite around the sample.<sup>9</sup> The thermodynamic model predicted the same amount of boron pickup for both the killed and unkilld samples.

Based on phase equilibria, thermodynamic calculations, and experimental results, the following mechanism is proposed. At 1585°C, the boron nitride thermally decomposes at the refractory interface according to **Equation 1**:



Boron and nitrogen dissolve into the steel. Some of the nitrogen diffuses to the molten pool where it recombines into nitrogen gas according to **Equation 2** and exits into the furnace atmosphere.



During solidification, the Fe- $\text{Fe}_2\text{B}$  eutectic liquid phase forms resulting in the microstructure observed in this study. **Equation 3** presents the formation of  $\text{Fe}_2\text{B}$  during solidification.



Iyengar and Pehlke proposed a similar dissolution mechanism in experiments on boron nitride dissolution in liquid iron.<sup>10</sup> In their study, pure iron was melted and a tablet of boron nitride dissolved into the melt. Gas from the furnace atmosphere was sampled. Iyengar and Pehlke detected

Table 2. Input for thermodynamic calculations for boron nitride samples

Sample	Fe (mol)	C (mol)	BN (mol)	Al (mol)	Ar (mol)	CO (mol)
Unkilld	49.993	0.007	1	-	0.99999	0.00001
Al-killed	49.925	0.007	1	0.0675	0.99999	0.00001

Table 3. Predicted mole fraction of phases in the liquid steel in the boron nitride samples

Sample	Fe	B	C	N	O	Al	AlO	BO	B <sub>2</sub> O	Al <sub>2</sub> O
Unkilld	0.98	0.020	0.0014	0.0095	$7.8 \times 10^{-8}$	-	-	$1.4 \times 10^{-8}$	$2.3 \times 10^{-9}$	-
Al-killed	0.98	0.020	0.0014	0.0095	$4.6 \times 10^{-8}$	0.0013	$7.0 \times 10^{-8}$	$8.0 \times 10^{-9}$	$1.3 \times 10^{-9}$	$9.4 \times 10^{-9}$

significant nitrogen gas evolution with the dissolution of the boron nitride pellet. The rate of gas evolution was reportedly affected by the original boron content of the iron, which is indicative of this type of dissolution mechanism.<sup>10</sup>

Zirconia depletion from the steel/refractory interface, as observed in **Figures 4 and 5**, was most likely caused by the dissociation of zirconia since no zirconia grains were observed in the steel. EDS analysis was not able to confirm the presence of dissolved zirconium in the steel of either sample.

### Silicon Carbide

Silicon carbide samples exhibited microstructures indicating a reaction between the steel (killed and unkilld) and the refractory. Large reaction zones at the interface were observed in both the unkilld (800  $\mu\text{m}$  thick) and aluminum-killd (500  $\mu\text{m}$  thick) samples (See **Figure 10**). Inside the reaction zone, a mixture of graphite, silicon carbide, and steel were detected. Steel was found in the reaction zone where it had penetrated the silicon carbide.

Both the killd and unkilld samples displayed similar microstructures after the experiments (see **Figure 11**). These samples are significantly different than the single phase ferrite observed in the original steel pins (**Figures 7 and 9**). After the experiments, the microstructure consisted of three phases, iron (light gray phase), graphite (dark gray-black phase), and FeSi (medium gray phase). The FeSi was identified by standard-less EDS as 46 at% Si and 54 at% Fe, within the detection limits for FeSi (50 at%). EDS determined the average overall steel composition for both samples to be 42 at% Si which is in the two-phase

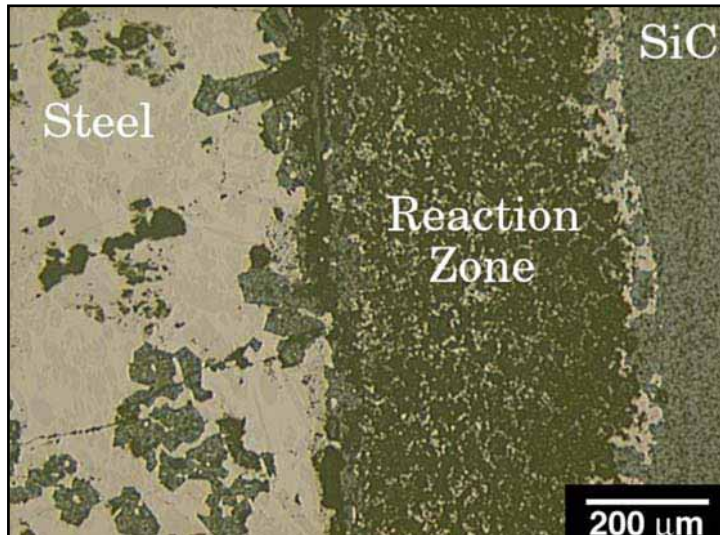


**Fig. 10.** RL image of the steel/SiC interface in the aluminum killed ULC steel sample.

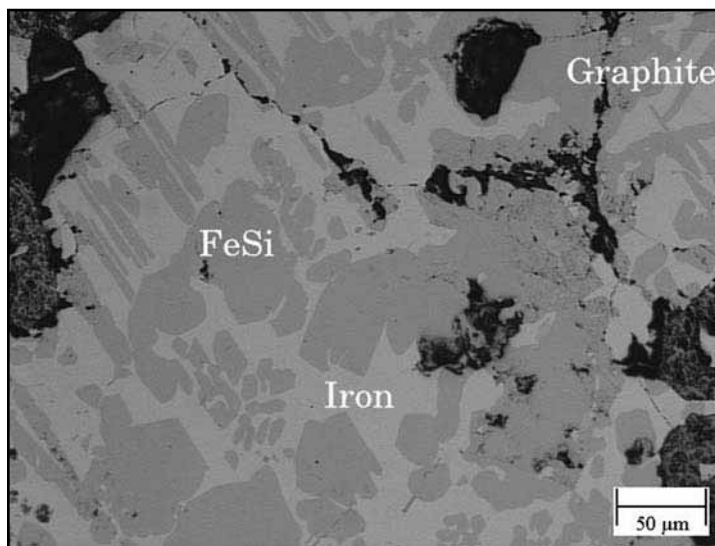


**Fig. 11.** RL image of aluminum killed ULC steel from the center of the SiC sample.

region consisting of  $\alpha$ -iron and FeSi in the iron-silicon system. XRD analysis of the steel and refractory confirmed the killd and unkilld samples contained FeSi in addition to iron, graphite, and silicon carbide.

Based on the observed ratio of steel to reaction layer in each sample, a molar ratio of 1:28 moles of silicon carbide to steel were used in FACTSage™ computations to determine the equilibrium species at 1585°C. **Table 4** lists the input moles for the model based on thermodynamic standard states, iron, carbon, aluminum and silicon carbide were input as solids and argon and carbon monoxide were input as gases. Results from the thermodynamic calculations are presented in **Table 5**. The carbon and silicon content of the steel was predicted to increase considerably. These predictions are consistent with the observed microstructure in both steel types.

In light of the microstructural characteristics, EDS analysis, XRD analysis, and thermodynamic calculation, a plausible mechanism for the observed behavior of the various samples is proposed. As steel penetrates the refractory, silicon carbide decomposes at 1585°C according to **Equation 4**.



Carbon, which appeared from the decomposition of silicon carbide, forms free graphite as observed in the microstructure. It should be noted that Pan et al. have observed that silicon carbide readily decomposes in the presence of transition metals.<sup>11</sup> This decomposition leads to graphite and metal silicide formation, as observed in these experiments. Silicon dissolves into the molten steel. Upon solidification,

**Table 4. Input data from thermodynamic computations for the silicon carbide samples**

Sample	Fe (mol)	C (mol)	SiC (mol)	Al (mol)	Ar (mol)	CO (mol)
Unkilld	27.996	0.00392	1	-	0.99999	0.00001
Al-killd	27.958	0.00392	1	0.0378	0.99999	0.00001

**Table 5. Predicted mole fraction of phases in the molten steel for silicon carbide**

Sample	Fe	Al	C	Si	O	SiO	AlO	Al <sub>2</sub> O
Unkilld	0.93	-	0.033	0.033	$1.2 \times 10^{-9}$	$1.2 \times 10^{-11}$	-	-
Al-killd	0.93	0.0013	0.033	0.033	$1.2 \times 10^{-8}$	$1.2 \times 10^{-11}$	$1.2 \times 10^{-9}$	$2.3 \times 10^{-10}$

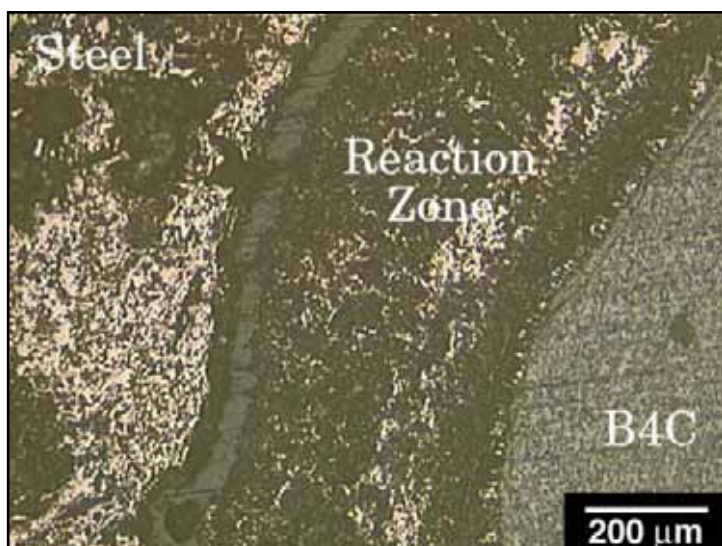


Fig. 12. RL image of aluminum killed ULC steel/BC interface.

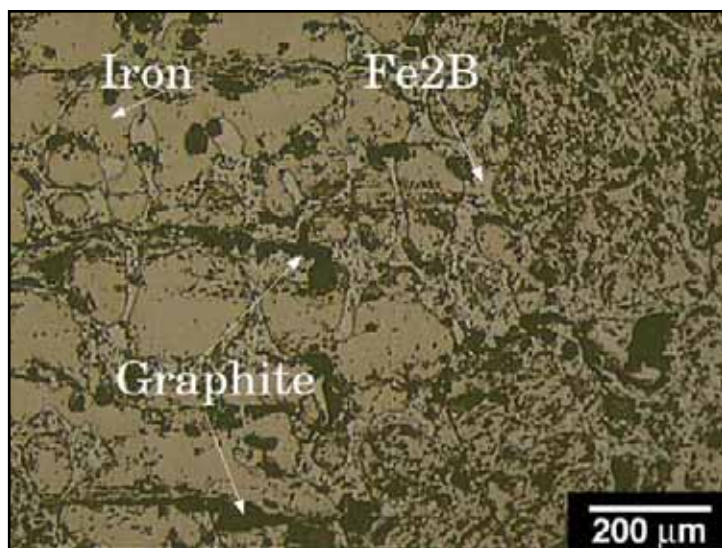


Fig. 13. RL Image of aluminum killed ULC steel from the center of the BC sample.

FeSi forms according to the phase equilibria involved in the iron-silicon system.

### Boron Carbide

Examination of the refractory/steel interface by RL revealed evidence of reactions between the steel and refractory. A reaction zone approximately 450 μm thick was observed in both the unkilld and aluminum-killd samples (See Figure 12). The similarity in reaction layer thickness indicates that the reaction was apparently unaffected by the aluminum content of the steel. Some steel and a considerable amount of graphite were found to be present in the reaction layer. In the steel, a mixture of graphite, iron, and a third phase were detected. XRD analysis of the steel and refractory confirmed the presence of graphite, iron and Fe<sub>2</sub>B in the samples, indicating that the carbon and boron from the boron carbide has dissolved in the steel.

Steel at the center of the sample also demonstrated the sign of the reaction between boron carbide and steel. Black graphite particles were observed throughout the unkilld and aluminum-killd steel samples (See Figure 13). The steel was also found to contain two different metallic phases. In Figure 13, the tan colored phase appears to be surrounded by a lighter colored phase. Based on the iron-boron phase diagram, the tan colored phase would be α-iron and the lighter phase Fe<sub>2</sub>B.

The microstructure observed in these samples was similar to the microstructures observed by Terry and Chinyamakobvu in work on an iron-boron carbide composite.<sup>12</sup> In their study, they determined that the boron and carbon from boron carbide dissolved into the liquid iron and formed Fe<sub>2</sub>B and graphite in the solidified material.

A molar ratio of 1:168 moles B<sub>4</sub>C to steel in the unkilld steel sample and a ratio of 1:188 moles for the aluminum-killd sample were used in FACTSage™ to predict the equilibrium species that formed during the experiment. These ratios were determined from the relative amount of steel and thickness of the reaction layer in each sample. Table 6 provides the input moles for the model based on thermodynamic standard states, iron, carbon, aluminum and B<sub>4</sub>C were input as solids and argon and carbon monoxide were input as gases. Computation results for equilibrium at 1585°C are presented in Table 7. The results predict boron and carbon pickup in the steel.

Based on the thermodynamic predictions, microscopy, and phase equilibria of the iron – boron system, it seems likely that the following reaction mechanism occurred during the experiments. Boron carbide at the refractory/steel interface thermally decomposed into boron which then dissolved into the steel, and graphite (see Equation 5).



Some of the carbon precipitated to form the graphite phase observed in the microstructure. During solidification, primary iron grains formed and Fe<sub>2</sub>B formed in the interdendritic regions.

Table 6. Input data from thermodynamic computations for the boron carbide samples

Sample	Fe (mol)	C (mol)	B <sub>4</sub> C (mol)	Al (mol)	Ar (mol)	CO (mol)
Unkilld	167.976	0.2352	1	-	0.99999	0.00001
Al-killd	187.718	0.2632	1	0.2538	0.99999	0.00001

Table 7. Predicted mole fraction of phases in the molten steel for the boron carbide samples

Sample	Fe	B	C	O	Al	AlO	BO	B <sub>2</sub> O	Al <sub>2</sub> O
Unkilld	0.97	0.023	0.007	4.2x10 <sup>-9</sup>	-	-	8.0x10 <sup>-10</sup>	1.7x10 <sup>-10</sup>	-
Al-killd	0.97	0.020	0.005	4.6x10 <sup>-9</sup>	0.0013	6.4x10 <sup>-9</sup>	8.0x10 <sup>-10</sup>	1.5x10 <sup>-10</sup>	8.8x10 <sup>-10</sup>

## CONCLUSIONS

The materials evaluated in this study reacted with molten steel. Boron nitride reacted with the steel contaminating the steel with boron and nitrogen, while some of the nitrogen may have exited to the surrounding atmosphere. Boron in the steel was sufficient to form Fe<sub>2</sub>B during solidification. Silicon carbide decomposed in the presence of molten steel forming free graphite and silicon which dissolved in the molten steel resulting in the formation of regions containing FeSi in the solidified steel. Steel and boron carbide reacted to form large amounts of Fe<sub>2</sub>B and free graphite in the microstructure. The most severe reaction between molten steel occurred with the silicon carbide and boron carbide refractories.

## ACKNOWLEDGEMENTS

This material is based on work supported by the U.S. Department of Energy, the American Iron and Steel Institute and member companies participating in the research under award number DE-FC07-97ID13554. Any opinions, findings, and conclusions or recommendations expressed in this material are those of the authors and do not necessarily reflect the views of the Department of Energy. The authors would also like to thank William Rowden and Jennie Tuttle for their assistance in conducting this research.

## REFERENCES

- <sup>1</sup>J. Poirier, B. Thillou, M. Guiban, G. Provost, *Mechanisms and Countermeasures of Alumina Clogging in Submerged Nozzles*, Proceedings 78th Steelmaking Conferences, Vol. 78, pp. 451-456, Iron and Steel Society, 1995.
- <sup>2</sup>S. Ogibayashi, "Mechanism and Countermeasure of Alumina Buildup on Submerged Nozzle in Continuous Casting", *Taikabutsu Overseas*, **15** [1] 3-14 (1994).
- <sup>3</sup>J. Poirier, D. Verrelle, B. Thillou, G. Provost, C. Taffin, P. Tassot, *Study of Clogging Phenomena in Continuous Casting Submerged Nozzles*, Proceedings of Unified International Technical Conference on Refractories, German Refractory Association, UNITECR '91 pp. 226-229, 1991.
- <sup>4</sup>Y. Fukuda, Y. Ueshima, S. Mizoguchi, "Mechanism of Alumina Deposition on Alumina Graphite Immersion Nozzle in Continuous Caster", *ISIJ Int.*, 164-168 (1992).
- <sup>5</sup>D. Richerson, *Modern Ceramic Engineering: Properties, Processing and Use in Design*, 2nd ed.; Marcel Dekker: New York, (1992).
- <sup>6</sup>K. Asano, A. Ishii, Y. Tsutsui, "Reactivity Between BN Composite Ceramics and Molten Stainless-Steel", *Taikabutsu Overseas*, **11** [3] 14-25 (1991).
- <sup>7</sup>I. Campbell, *High Temperature Technology*. John Wiley & Sons Inc., New York. (1956)
- <sup>8</sup>L. Trueba, K. D. Peaslee, and J. D. Smith, "Nozzle Clogging During the Continuous Casting of Aluminum-killed Steel", Doctoral Dissertation, University of Missouri-Rolla, Rolla, MO, 2003.
- <sup>9</sup>S. Ramachandran, K. D. Peaslee, J. D. Smith, "Thermochemistry of Steel-refractory Interactions in Continuous Casting Nozzles", *Iron and Steelmaker (ISS Transactions)*, 30 55-65 (2003).
- <sup>10</sup>G. Iyengar, R. Pehlke, "Dissolution of Boron Nitride in Liquid Iron", *Metall. Trans.*, **1** 2235-2242 (1970).
- <sup>11</sup>Y. Pan, J. Baptista, "Chemical Instability of Silicon Carbide in the Presence of Transition Metals", *J. Am. Ceram. Soc.*, **79** [8] 2017-2026 (1996).
- <sup>12</sup>B. Terry, O. Chinyamakobvy, "Assessment of B<sub>4</sub>C Reaction With Liquid Iron Alloys", *J. Mater. Sci.*, **29** [2] 464-467 (1994).